Available online at www.sciencedirect.com

ScienceDirect

Biochimica et Biophysica Acta 1757 (2006) 1096–1109

BIOCHIMICA ET BIOPHYSICA ACTA

BBA

www.elsevier.com/locate/bbabio

Electron tunneling chains of mitochondria

Christopher C. Moser *, Tammer A. Farid, Sarah E. Chobot, P. Leslie Dutton

The Johnson Research Foundation, Department of Biochemistry and Biophysics, University of Pennsylvania, 1005, Stellar-Chance Laboratories, 422, Curie Boulevard, Philadelphia, PA 19104-6059, USA.

Received 30 January 2006; received in revised form 11 April 2006; accepted 13 April 2006
Available online 5 May 2006

Abstract

The single, simple concept that natural selection adjusts distances between redox cofactors goes a long way towards encompassing natural electron transfer protein design. Distances are short or long as required to direct or insulate promiscuously tunneling single electrons. Along a chain, distances are usually 14 Å or less. Shorter distances are needed to allow climbing of added energetic barriers at paired-electron catalytic centers in which substrate and the required number of cofactors form a compact cluster. When there is a short-circuit danger, distances between shorting centers are relatively long. Distances much longer than 14Å will support only very slow electron tunneling, but could act as high impedance signals useful in regulation. Tunneling simulations of the respiratory complexes provide clear illustrations of this simple engineering.

Keywords: Mitochondria; Cytochrome *c* oxidase cytochrome bc1; Succinate dehydrogenase; NADH-ubiquinone oxidoreductase; Electron and nuclear tunneling; Oxidoreduction catalytic transformation; Energy conversion

1. Introduction

Fig. 1 presents the mitochondrial respiratory electron transfer chain comprising four transmembrane oxidoreductases that together convert redox potential free-energy between the reducing substrates NADH and succinate and the oxidizing substrate dioxygen into an electrochemical free-energy gradient of protons ($\Delta\mu_{H^+}$), the energy currency used to drive mitochondrial and cellular functions. This paper addresses the large sections of linear chains of redox cofactors evident in X-ray structures of each the four major membrane protein complexes. These cofactor chains extend over tens of Ångstroms within each protein complex to link remote catalytic sites of multi-electron substrate oxidation-reduction. In cytochrome *c* oxidase (complex IV) and cytochrome bc_1 (complex III), the redox chains direct electrons across the membrane and contribute to $\Delta\mu_{H^+}$, while in succinate dehydrogenase (complex II) and NADH-ubiquinone oxidoreductase (complex I) the chains extend out of the membrane to well removed catalytic sites. This paper explores the application of our empirically established electron tunneling expressions to these cofactor chains of respiratory complexes. The electron tunneling expressions, derived and tested with photosynthetic reaction center proteins, and backed up by statistics from a growing family of oxidoreductases, clearly demonstrate that cofactor chains of respiratory energy conversion protein complexes adhere to the same tunneling design guidelines as those of photosynthetic proteins. The expressions thus offer a simple way of examining the tunneling parameters that underpin the activity of respiratory protein cofactor chains including the calculation of parameters that for respiratory proteins may be experimentally out of reach. The work also reveals the critical role of high electron tunneling rates at the interface of simple electron tunneling cofactor chains and the sites of multi-electron substrate oxidation-reduction where bond breaking and bond forming take place and where primary energy conversion occurs.

2. Electron tunneling equations

In a successful intraprotein electron tunneling rate expression [1], four parameters are more than sufficient to provide

* Corresponding author. Tel.: +1 215 573 3909; fax: +1 215 573 2235.
E-mail address: moserc@mail.med.upenn.edu (C.C. Moser).

0005-2728/$ - see front matter © 2006 Elsevier B.V. All rights reserved.
doi:10.1016/j.bbabio.2006.04.015

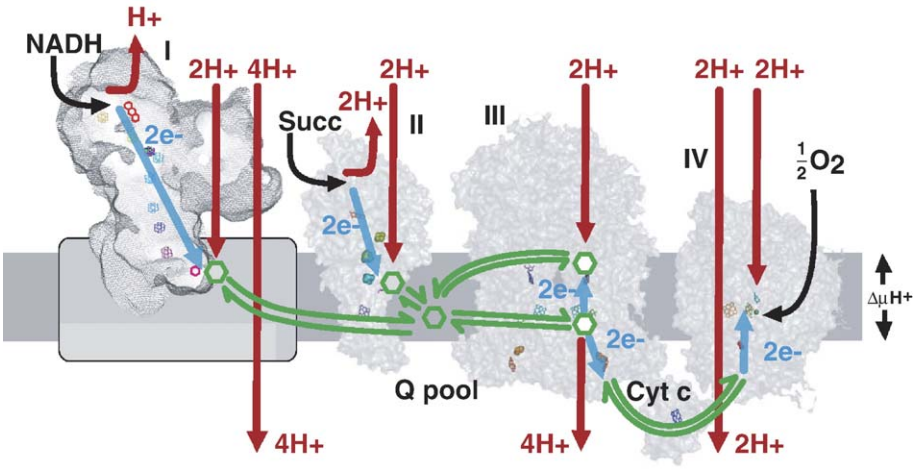

Fig. 1. The membrane bound mitochondrial respiratory Complexes I through IV. Protein outlines for Complex I is from Hinchcliffe et al. [51]; other cofactor positioning taken from structures referenced in later figures. Complex III is shown as a functional dimer. Diffusing elements quinone and cytochrome *c* [59] connect the complexes. In electron transfer of two electrons from NADH to O_2, 10 protons are released to the outside of the mitochondrion while 11 are removed from the inside. However, when NADH is formed from NAD^+ in the citric acid cycle inside the mitochondrion, a proton is released. Thus, a net 10 protons are removed from the inside and moved to the outside as NADH is formed and its electrons transferred to O_2.

tunneling rate estimates given the uncertainty of measurement of both the parameters and the rates.

$$\log k_{et}^{exer} = 13-(1.2-0.8\rho)(R-3.6)-3.1\frac{(\Delta G^o+\lambda)^2}{\lambda} \quad (1)$$

This equation is based on an exponential dependence of electron tunneling with distance (R in Å) through an insulating protein barrier, where the height of the tunneling barrier depends on how vacuum-like or how bond-like the intervening protein medium is. An elementary structure-based estimate that roughly correlates with effective barrier height is the packing density (ρ) which is around 0.76±0.1 in a typical protein. Marcus realized that electron tunneling often has a Gaussian dependence of rate vs. distance [2], with a maximal possible rate when the driving force ($-\Delta G°$ in eV) matches an energetic term called the reorganization energy (λ in eV). Together $\Delta G°$ and λ determine the activation energy for the electron tunneling. The reorganization energy can be thought of as the energy required to move the nuclei of the redox cofactors and their surroundings from an equilibrium configuration favored when the electron is on the donor, to the equilibrium geometry favored when the electron is on the acceptor, but constraining the electron to remaining on the donor.

Marcus' expression was based on a classical model in which the potential energy surfaces of the reactant (reduced donor and oxidized acceptor) and product (oxidized donor and reduced acceptor) were intersecting, parabolic, simple harmonic oscillator wells, with the reaction coordinate being a generalized one of nuclear vibration/reorganization that carried the reactant equilibrium geometry into the product equilibrium geometry. In the Marcus classical view, the vibrations coupled to electron transfer are all of low enough energy that a non-quantized harmonic oscillator description is sufficient. Work with photosynthetic reaction centers over a wide range of cryogenic temperatures [3] has shown that the Marcus classical expression is not as appropriate as an expression that uses vibrations coupled to electron transfer that have an energy higher than Boltzmann kT at room temperature. Indeed, the weighted characteristic frequency of vibration coupled to electron transfer in reaction centers appears to be close to 0.06 eV, larger than the Boltzmann room temperature energy of about 0.025 eV [4]. An expression that allows this quantized vibrational frequency but maintains a Gaussian free energy dependence of rate has been described by Hopfield [5]. Although this characteristic frequency is rather difficult to access experimentally and may vary from one electron tunneling reaction to another, the generic value appears to give reasonable estimates of electron transfer rates in many cases. The somewhat broader quantized version of the Gaussian dependence of rate on free energy gives rise to the 3.1 coefficient in the room temperature expression of Eq. (1). The corresponding classical Marcus expression would have a coefficient of 4.2.

Eq. (1) relates to exergonic electron transfer reactions. Many electron tunneling reactions in biology are uphill. One way to estimate the rate of an uphill electron tunneling reaction is to use Eq. (1) to calculate the corresponding down hill electron transfer of the reverse reaction and then, assuming the forward and reverse rates are related by a Boltzmann energy term, slow the forward tunneling rate by an order of magnitude for every 0.06 eV of uphill $\Delta G°$.

More austere tunneling expressions with fewer parameters are often quite useful, and the only choice when there is a lack of experimental information. Packing is the easiest parameter to replace with a generic value, since it rarely has a dominant effect. This leads to a three-parameter expression:

$$\log k_{et}^{exer} = 15-0.6R-3.1\frac{(\Delta G^o+\lambda)^2}{\lambda} \quad (2)$$

The 0.76 packing typical of protein leads to the 0.6 coefficient in front of the R. This corresponds to a natural base exponential coefficient of decay with distance (β) of 1.4 $Å^{-1}$.

The next parameter to consider replacing with a generic value is reorganization energy, both because it is rarely measured with any precision, and because it does not appear to be

Table 1
Estimates of single-electron redox center potentials in respiratory complexes

Mitochondrial complex	Redox center	Em_7	Reference
I	N1a	−0.38	[48,63]
	N1b	−0.25	[48,63]
	N2	−0.10	[48,63]
	N3	−0.25	[48,63]
	N4	−0.25	[48,63]
	N5	−0.25	[48,63]
	N6a	−0.25	[66]
	N6b	−0.25	[66]
II	[2Fe2S]	0.00	[68]
	[4Fe4S]	−0.260	[68]
	[3Fe4S]	0.06	[69]
	heme	−0.185	[70]
III	c_1	242	[23]
	FeS	280	[64]
	b_L	−50	[32]
	b_H	80	[32]
IV	Cu_A	.24	[65]
	a	0.26	[16]
	Cu_B	0.28 (0.32)	[16]
	Tyr	1.0	[67]

engineered/naturally selected to have non-generic values in the respiratory complexes. ~0.7 eV seems to be an adequate generic value, and leads to a two-parameter expression which may be the most useful when examining many of the large number of electron transfer protein structures now available.

$$\log k_{et}^{exer} = 15 - 0.6R - 3.1\frac{(\Delta G^o + 0.7)^2}{0.7} \quad (3)$$

When bond making and breaking takes place at catalytic sites, the assumptions underlying these non-adiabatic tunneling expressions are no longer valid, and non-electron tunneling barriers become important. However, formally, we can accommodate the larger barriers at catalytic sites with larger "effective" reorganization energies which, together with driving force, define the activation energy for electron transfer. Thus, by adjusting an effective reorganization energy and/or driving force, the tunneling equations can mimic essentially non-tunneling electron transfer reactions at catalytic sites with rates that are consistent with the observed rate of catalysis. By including appropriate rates at catalytic sites in electron tunneling network simulations, it is then possible to see the relative importance of other truly electron tunneling limited rates in the tunneling network.

The most extreme and simplest tunneling expression retains only distance as a parameter, setting the driving force to a generic value of zero, since most biological electron transfer reactions have little driving force.

$$\log k_{et} = 12.8 - 0.6R \quad (4)$$

This sort of equation would be appropriate only if there is a great deal of ignorance about the electron transfer system, which fortunately does not apply to the respiratory complexes.

2.1. Cofactor redox midpoint potentials estimates

It is now possible to apply these equations in useful simulations of electron tunneling through the respiratory complexes, with the benefit of crystal structures that resolve redox cofactors and allow estimates of edge-to-edge distance, and also decades of work trying to define redox midpoint potentials that can be used to estimate the driving force for electron transfer. Together, these provide the two most important parameters for the tunneling expressions.

It is true that experimental equilibrium redox midpoint potentials (Tables 1 and 2) may not be entirely appropriate to estimate the driving force for electron tunneling from one particular redox microstate of a multi-redox center respiratory complex to another, especially if redox centers are so close that electrostatic interactions between them can noticeably shift the affinity of the redox centers for an electron. Nevertheless, equilibrium redox midpoint values (E_m values) provide a good place to start simulations and begin to reveal the overall engineering of the tunneling systems of the respiratory complexes in action. These tunneling simulations illustrate the far reaching rule of distance in electron transfer protein design. Crystal structure derived distances and (when used) packing densities will appear in colored structural figures placed just before each panel of simulations for each complex. Redox midpoint potentials used to estimate driving forces are given in Tables 1 and 2.

2.2. Complex IV: cytochrome c oxidase

Many of the electron transfers within cytochrome *c* oxidase (Fig. 2) take place faster than the rapid mixing of oxygen or

Table 2
Estimates of multi-electron redox center potentials in respiratory complexes

Mitochondrial complex	Redox center	Em_7 ave (V)	log K_{stab}	Em_7 1st reduction	Em_7 2nd reduction	Reference
I	FMN	−0.34	−1.6	−0.389	−0.293	[71]
energized (+uncoupler)	Qn	−0.06 (0.06)	2	0	−0.12 (0.12)	[49]
II	Flavin	−0.079	−1.6	−0.127	−0.031	[72]
	Qs	0.134	−1.3	0.096	0.172	[73]
III	Qo	0.09	−16	(−0.39)	(0.57)	this work
	Qi	0.14–.018	−2.3	0.02–0.07	0.26–0.29	[23]
IV reduced (mixed val.)	a_3			0.6	0.28 (0.32)	[16]
	O_2	0.81[8]		−0.27	0.93	this work
	O_2			0.33	2.25	this work

For two electron redox centers, individual redox midpoint potentials for the first and second reduction is related to a semiquinone stability constant K_{stab} (see Eq. (5)). For heme a_3, the $Fe^{II/III}$ and $Fe^{III/IV}$ estimates are reported, while for O_2, we report the values in aqueous solution [8] slightly moderated (by 5%) towards the average value of 0.81 V.

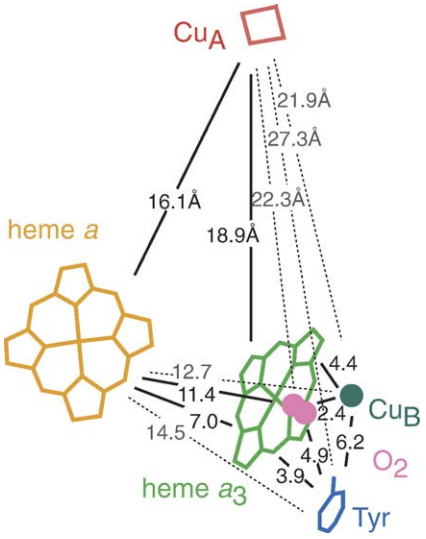

Fig. 2. Edge-to-edge cofactor distances in bovine cytochrome *c* oxidase, PDB crystal structure 1OCC [60]. Because O_2 is not stably bound in crystal structures, the corresponding distances with carbon monoxide in PDB crystal structure 1OCO [61] are shown.

cytochrome *c* with oxidase in stopped-flow spectrometers. Fortunately, it has been possible to resolve the rapid electron transfers within the oxidase itself by taking advantage of the fact that carbon monoxide can be stably bound to the heme a_3 of the reduced Cu_B-heme a_3 binuclear center. After O_2 is leisurely mixed with the CO-ligated oxidase in the dark, CO can be rapidly photolyzed. This allows O_2 to diffuse and bind to heme a_3 on a ~10 μs timescale and initiate a series of electron transfers. The delivery of 4 electrons and the breaking of the O − O bond in O_2 reduction by the fully reduced oxidase is essentially complete in 30 μs [6]. The required electrons are obtained from Cu_B and heme a (one each) and from heme a_3, (two electrons) oxidizing it to the ferryl state. This is called the Pr state. Subsequently, Cu_A reduces heme a on the 0.1-ms timescale [7], and the heme a_3 ferryl state is reduced on a 1-ms timescale.

The electron tunneling times between the various reduced redox centers of the catalytic cluster and oxygen depend not only on distance, but also on driving force, especially when the reaction is uphill. The appropriate midpoint potentials for the redox couples of O_2 and its various partly reduced intermediates when bound at the bi-nuclear center are not known. It seems likely that the protein environment contributes to catalysis by leveling out the wide ranging redox potentials for O_2 in aqueous solution [8]. Fig. 3A illustrates the unlikely extreme case in which the protein environment completely levels out the redox couples to the 0.81-V average. If we disregard the experimental limitation that O_2 requires about 10 μs to diffuse to the catalytic cluster after CO photolysis and imagine that O_2 is already bound to the reduced oxidase, then the short distances between redox centers and the absence of large uphill driving forces would lead to inherent femtosecond to nanosecond tunneling rates in the successive oxidation of heme a_3 Fe^{II}, Cu_B, heme a_3 Fe^{III} and finally heme a. These rates are much faster than the observed 30 μs for oxygen reduction. More reasonable numbers for the oxygen redox couples introduce a significantly endergonic rate limiting-first step of O_2 reduction by heme a_3. Indeed, if the O_2 redox couples are similar to those in aqueous solution, moderated only 5% towards the average value by the catalytic site, then electron tunneling simulations with generic reorganization energies would match the experimentally observed oxygen reduction and O − O bond breaking rate.

It is believed that the heme a to heme a_3 electron transfer may be crucial for the energy coupling between the electron transfer and proton pumping functions of cytochrome oxidase [9] and that electron transfer directly from Cu_A to heme a_3 or other members of the immediate catalytic cluster may represent a possible energy wasting short-circuit reaction. The naturally selected distances between redox centers in oxidase by themselves work to assure that electron transfer from Cu_A progresses through heme a. Cu_A is 2.8Å closer to heme a than heme a_3, which would lead to a ~50-fold faster rate in a typically packed protein (Eq. (3)). In addition, it appears that the protein between Cu_A and heme a is somewhat more densely packed than the protein between Cu_A and heme a_3 (ρ of 0.87 compared to 0.79). Although it is not clear that this packing density difference has been naturally selected, Eq. (1) suggests that it adds an extra factor of 5 in favor of electron transfer from Cu_A to heme a over heme a_3. There is another way in which naturally selected distances between cofactors may work to prevent this potential short-circuit reaction. Reduction events at the catalytic cluster are likely to involve some energetically significant reorganization, such as movement of protons or reorientation hydrogen bond patterning. These extra activation barriers act somewhat like a large "effective" reorganization energy. This will slow all electron transfers to heme a_3, including the potentially harmful Cu_A to heme a_3 direct electron transfer.

A convenient way to isolate the potentially short-circuiting Cu_A to heme a_3 reaction and assess the effects of changing the activation energy for reduction of the catalytic cluster, is to remove heme a from the electron tunneling simulation (Fig. 3B). Analytical removal of a cofactor is similar to the experimental genetic knock-out of a cofactor, as has been done with heme b_H cofactor in complex III [10]. With a default reorganization energy of 0.7 eV, we would expect 30 μs reduction of O_2, with double oxidation of heme a_3 and oxidation of Cu_B. Because there is no heme a to provide the fourth electron, we expect to see the oxidation of a nearby tyrosine. After the initial reactions, Cu_A to heme a_3 direct electron transfer would be slightly faster than a millisecond (dashed lines). Increasing the effective reorganization energy of catalytic cluster reduction to 1.5 eV slows the putative short-circuit to more than 100 ms (solid lines). This would correspond to an activation energy for cluster reduction of about 3–4 kcal/mol. When the heme a is put back (Fig. 3C), the short 7Å distance between heme a and heme a_3 means that electron transfer from a to a_3 will still be faster than O_2 reduction, even with the large effective reorganization energy for catalytic cluster reduction. Fig. 3C shows that tunneling limited oxidation of CuA on electron transfer to heme a takes place on the experimentally observed 0.1 ms timescale. However, following electron tunneling between heme a and the ferryl heme a_3 will be just as rapid in the simulation, in contrast to the slower 1 ms timescale observed experimentally. It is likely that still other energetic barriers, such as proton movement into the catalytic cluster to allow changes in heme a_3 ligation during reduction of

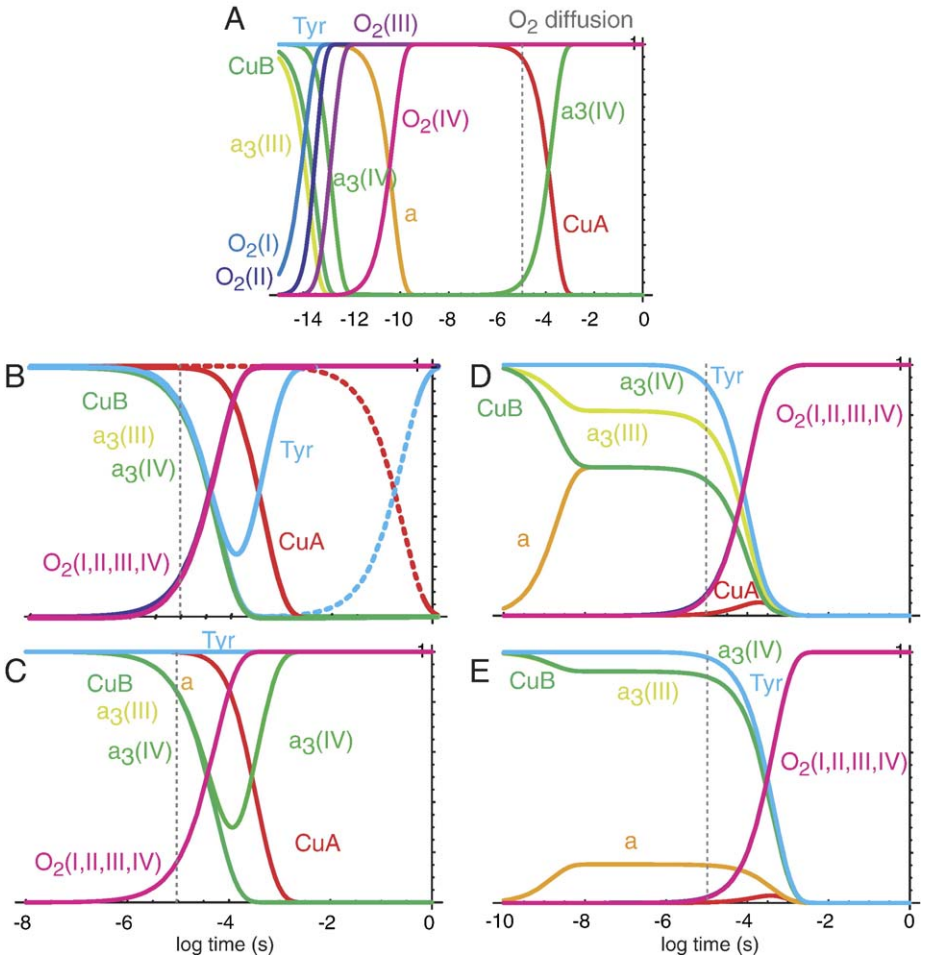

Fig. 3. Cytochrome oxidase tunneling network simulations. (A) Idealized electron tunneling simulation of fully reduced cytochrome oxidase reacting with bound O_2, where each O_2 redox couple has the average 0.81V E_m value. All other panels use O_2 redox couples close to those in aqueous solution, moderated on 5% towards the average value by the protein environment. Dashed line represents rate limiting O_2 diffusion time in practical photolysis experiments. (B) Tunneling simulation of a heme a knock out, showing that increasing the reorganization energy for electron transfer to the catalytic cluster from the default 0.7 eV value to 1.5 eV (dashed) can slow Cu_A to catalytic cluster "short-circuit" as much as required. (C) With heme a restored, the short heme a to a_3 distance means the large reorganization energy for electron transfer with the catalytic cluster does not slow oxygen reduction significantly. (D) Simulation of the mixed valence state using the average E_m values of Tables 1 and 2. (E) Simulations of the mixed valence state reaction with O_2 match experiment better when using the slightly elevated experimental E_m values for heme a_3 and Cu_B when heme a and Cu_A are oxidized.

the ferryl state, slow down the inherently fast inter-heme tunneling rates.

Another common way that rapid electron transfer within cytochrome oxidase is observed begins with CO bound to the mixed-valence state, in which only heme a_3 and Cu_B of the catalytic cluster are reduced, but heme a and Cu_A are oxidized. Under these conditions oxygen reduction is about ten times slower, and the fourth electron appears to be extracted in the end from a tyrosine at the catalytic cluster. This is the Pm state. For many years the 3 ms electron equilibration between nearby oxidized heme a and reduced heme a_3 immediately after CO photolysis of the mixed valence state [11,12] was taken as evidence that the tunneling equations presented here, which predict much faster nanosecond rates of electron tunneling, were not valid [13]. Recently, reexamination of this reaction at faster time resolution has provided evidence that the electron transfer is indeed the expected nanoseconds [14,15]. Fig. 3D illustrates the expected electron transfers after CO photolysis from the mixed valence state, including the nanosecond back equilibration with heme a and oxidation of the tyrosine. However, the rate of oxygen reduction is very similar to rate with the fully reduced state, and not an order of magnitude slower, as observed experimentally for the mixed valence state. If the redox midpoint potentials of heme a_3 and Cu_B are only 30 mV higher in the mixed valence state compared to the fully reduced state, as has been described in terms of electrical interactions of close redox centers [16], then the rate of the mixed valence simulations is close to that of experiment (Fig. 3E).

Cytochrome oxidase provides a clear example of how distance is used to manage electron transfer in engineering the efficient energy transducing function of oxygen reduction and proton pumping. A catalytic cluster with electron transfer distances of 5Å or less is assembled for the required number of redox centers for the catalytic reaction. For oxygen reduction this is four electrons using one two-electron redox center heme a_3, and two one-electron redox centers, Cu_B and tyrosine. These short distances mean that when inherently fast electron tunneling rates meet the energetic barriers associated with the bond making and breaking of catalysis, the net

result is rapid enough electron transfer to support the required millisecond catalytic turnover of respiration. Because O_2 seems only capable of binding to heme a_3 when heme a_3 and Cu_B are both reduced, oxidase has found a way to assure that four electrons will be available for reduction and that potentially destructive oxidizing intermediates are minimized. The placement of heme a only 7Å from the catalytic cluster is close enough to assure that electron transfer into the cluster will be rapid, even if there are energetic barriers imposed by the electron transfer coupled proton pumping function of oxidase. This short-distance, rapid electron transfer also may help to control the potential reactivity of the tyrosine radical by quickly reducing it in productive, energy-coupled electron transfer, although under physiological conditions in which electron delivery to the oxidase by cytochrome *c* is limiting, the tyrosine radical should persist until the cytochrome *c* arrives which could take as long as 100 ms. Furthermore, the placement of Cu_A 2.8Å closer to heme a than heme a_3 means that simply based on distance nearly all electrons will pass from Cu_A to heme a on the way to the catalytic cluster and be available for coupling to proton movement. Any additional energetic barrier associated with catalytic cluster reduction should slow direct electron tunneling and potential short-circuit danger between Cu_A and heme a_3 still further, while maintaining relatively rapid proton coupled electron transfer between heme a and heme a_3, at least until the back pressure from the transmembrane proton gradient becomes quite high.

2.3. Complex III: cytochrome bc1

Physiologically productive electron transfer in Complex III (Fig. 4) oxidizes reduced ubiquinone (QH_2) at the Qo site, releasing two protons to the exterior aqueous phase and reducing cytochrome *c*, the substrate for complex IV. Rather than simply connecting QH_2 oxidation at Qo to reduction of cytochrome *c* through a simple high potential chain (FeS and cyt c_1 redox centers), the design of complex III connects the Qo site to an additional, low potential chain, comprised of low and high potential b hemes (b_L and b_H) and a quinone reduction site at the opposite side of the membrane, Qi [17,18]. Thus, quinone oxidation at the Qo site sends one electron down the high potential chain to cyt c, while shunting the other electron down the low potential chain to reduce quinone at the Qi by one electron. This can be seen in the electron tunneling simulation of Fig. 5A. Transmembrane electron transfer down the low potential chain electrically charges the membrane while quinone reduction at Qi takes up protons from the transmembrane aqueous phase. By the time a second QH_2 oxidation at Qo has reduced another cyt c, the quinone at the Qi has been fully reduced and is released into the quinone pool. The net effect of two turnovers at the Qo site is oxidation of one QH_2 and reduction of two cyt c with energy transduction of redox energy into transmembrane proton and electron transfer, adding to $\Delta\mu_{H^+}$ (Fig. 1).

Unlike cytochrome oxidase, complex III operates under relatively little driving force and is fully and readily reversible [10,19]. This reversibility exposes complex III to the possibility of several semiquinone mediated short-circuit electron transfers [10], for example between the low and high potential chains, which would have the effect of undoing the elegant energy transduction made possible by divergent electron transfer down the high and low potential chains. Qi, has a relatively stable

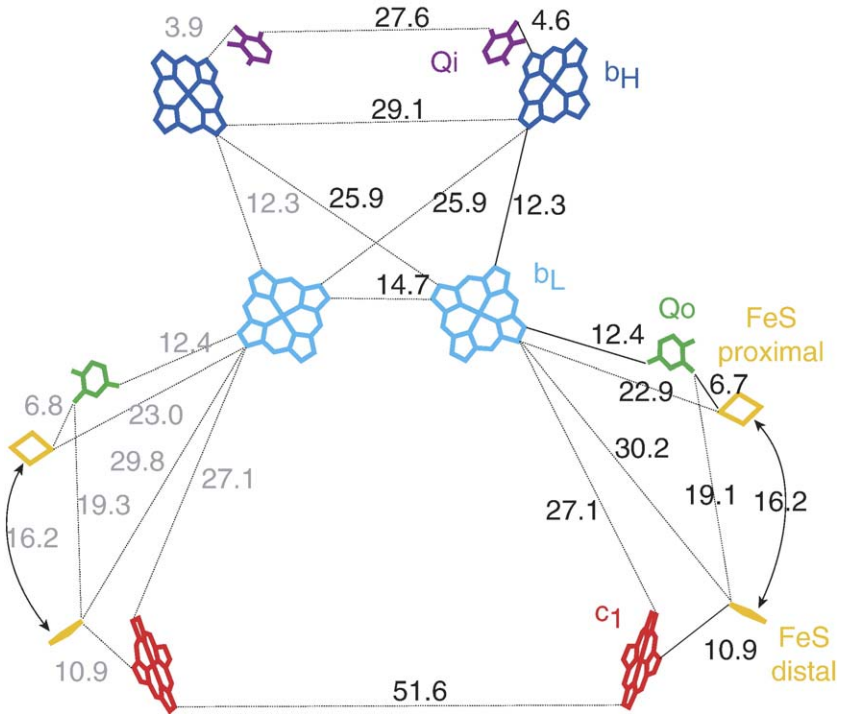

Fig. 4. Edge-to-edge distances and packing densities between pairs of redox cofactors in the dimer of Complex III as derived from the PDB structure 3BCC of avian cytochrome bc_1 [30]. The FeS cofactor is found in different positions in different crystal structures; here we show FeS proximal (3BCC) and distal (1BE3) [28] to the Qo site. As a crystal structure with ubiquinone in the Qo site is not available, the ring of inhibitor stigmatellin is used as a substitute to estimate distances.

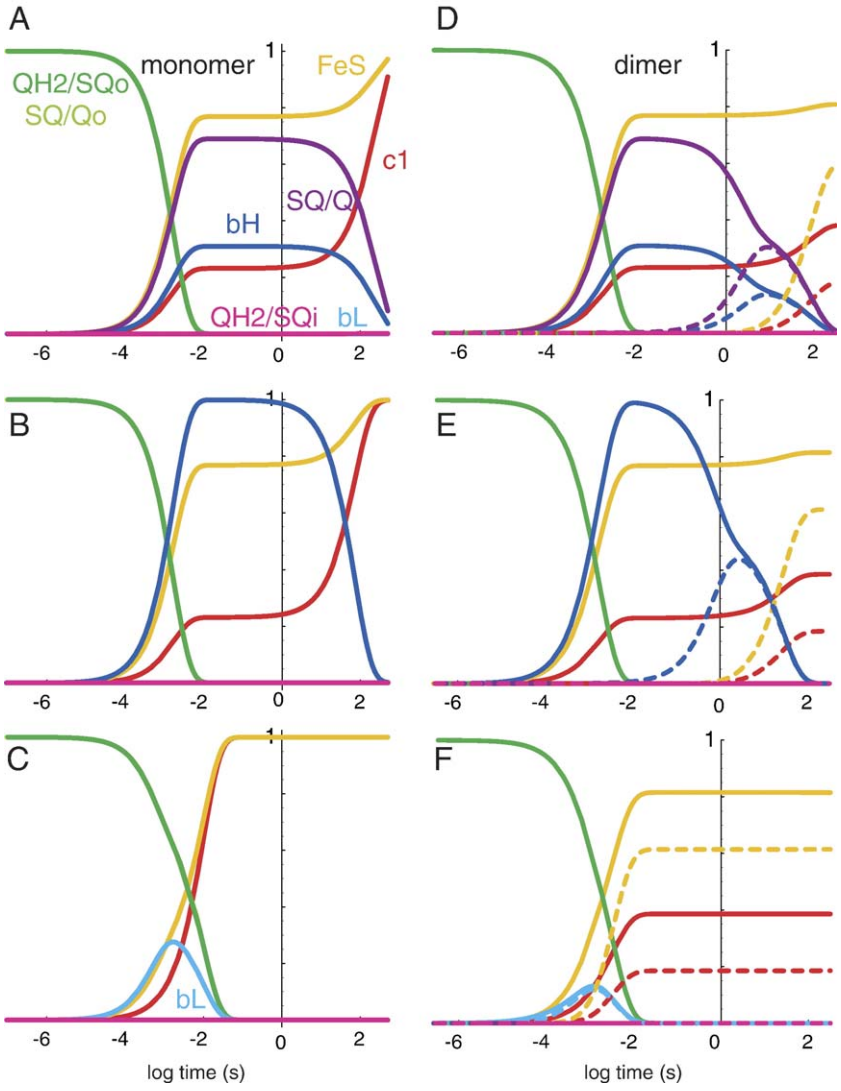

Fig. 5. Electron tunneling simulations of oxidized Complex III reacting with a single reduced quinone at a Qo site. Simulations of monomers with electron tunneling within halves of the dimer are shown on the left. Simulations with expected electron tunneling between dimer redox centers, especially between closest approaching hemes b_L are shown on the right, with dashed lines for occupancy of reduced states of the second half of the dimer that had oxidized Qo quinone to begin with. (A and D) All redox centers included. (B and E) Qi knock-out, simulating the removal of Qi with an inhibitor such as antimycin. (C and F) Heme b_H knockout, simulating site directed mutants that do not incorporate heme b_H [10]. Simulations do not include a gating of the redox states of Qo, hence short-circuits are expected between the high and low potential chains and visible in the simulations as the final reoxidation of hemes b and Qi and reduction of FeS and heme c1. Short-circuits in the b_H knock-out are severe enough to be comparable to the catalytic quinone oxidation rate.

semiquinone, easily observed at alkaline pHs [20,21], However, Qo has an unstable semiquinone that has never been observed. It is possible that Qo oxidation and reduction takes place through a two-electron concerted reaction [10], in which a semiquinone state is present so fleetingly (e.g., femtoseconds) that it never relaxes into a true intermediate state. Such a mechanism would neatly avoid the short-circuit threat. However, it is commonly believed that semiquinone exists as a brief but real intermediate in Qo site catalysis [22]. If so, then the electron transfer engineering must allow the semiquinone to be sufficiently accessible to enable rapid forward and reverse catalysis, but not so accessible so as to foster short-circuits.

One measure of the redox couples of a quinone relevant to the observability of a semiquinone is the stability constant, K_{stab}. If the oxidized, semiquinone and reduced quinone were in redox equilibrium, then

$$K_{stab} = \frac{[SQ]^2}{[Q][QH_2]} = 10^{(E_mSQ/QH_2 - E_mQ/SQ)/0.06} \quad (5)$$

Stability constants of greater than one mean that the semiquinone is a dominant species during a redox titrations, while log K_{stab} <-4 means that semiquinone will be barely observable, if at all. The redox couples and stability constant for Qi have been measured (log K_{stab} is ~ -2.3 at neutral pH) [23], but the stability constant for Qo is small and unknown. Because the oxidized and reduced quinone appear to bind equally at the Qo site [24], the average of the Qo redox couples should be

similar to that of the quinone pool, 0.09 V at neutral pH [25]. Because the SQo has not been observed by EPR, the log stability constant should be less than −7 [22,26]. Fig. 5 shows that a log K_{stab} for Qo of −16 will lead to electron tunneling reactions that match the observed rates, using the generic 0.7 eV reorganization energy of Eq. (3) and using quinone analogue inhibitor stigmatellin to estimate the position of ubiquinone, which has so far not been crystallized in the Qo site.

Fig. 5A shows the case of all components oxidized except for Qo, with the 10^{-16} K_{stab} providing for millisecond catalysis of quinone oxidation. This is an even lower K_{stab} than the 10^{-10} indicated by Mitchell for free quinone in the membrane pool [27]. FeS is modeled as moving between two sites, distal and proximal to the Qo site, as shown in various crystal structures [28–30], with a rate of about 10^5 s^{-1} [31]. Heme b_L is only transiently reduced as the electron comes to reside on heme b_H and Qi. Here we have been using universal midpoint potentials and ignoring the redox midpoint influencing interactions between the redox states of Qi and heme b_H. These interactions have been the subject of many conflicting reports[20,32–34] and will be addressed by us in a future report. When the electron can get as far as Qi, short-circuit through reverse reactions and SQo is safely slowed to a minute timescale. These simulations use equilibrium redox potentials without considering the transmembrane potential. Under physiological conditions, the $\Delta\mu_{H^+}$ will tend to disfavor Qi reduction and back up the electrons onto the hemes b.

When the redox center Qi is knocked-out in the simulation, analogous to the experimental case in which Qi inhibitor antimycin is added (Fig. 5B), the heme b_H reduction is dominant, with short-circuits still taking place relatively slowly on the order of tens of seconds timescale under non-membrane-energized conditions. However, when heme b_H is knocked-out, as has been done genetically [10], then in these simulations the electron cannot escape from heme b_L and is prone to millisecond short-circuit reactions that are comparable to the rate of catalysis. Because rapid short-circuit reactions are not observed experimentally in heme b_H knock-outs, Qo site catalysis was proposed to be either a concerted mechanism or a double-redox gated mechanism [10,35], in which the redox couples of Qo and the stability constant were modulated to allow catalysis in certain redox states, but to make the semiquinone inaccessible in others.

Complex III is a dimer. Indeed, the FeS subunit from one dimer reaches across the dimer interface and interacts exclusively with the heme Qo site of the other half. With a heme b_L edge-to-edge spacing of 14.7Å (Fig. 4), functionally significant electron tunneling between halves of the dimer is to be expected. This is shown in Fig. 5D–F, as the dimer kinetics corresponding to the monomer wild-type and knock-outs of panels A–C. Redox equilibration of the low potential chains is expected to take tens of seconds or seconds, depending upon the activity of Qi. Short-circuit reactions occur in both halves of the dimer, even though reduced quinone has been introduced to only one of the Qo sites. However, with the same fixed stability constant of 10^{-16}, the heme b_H knockout allows the electron to linger on heme b_L, with cross-dimer redox equilibration on the millisecond timescale of catalysis, and both sides of the dimer short-circuit on this same timescale. These simulations show that electrical contact across the dimer interface is significant on the catalytic timescale, and that in a certain sense, by acting as a functional dimer, Complex III has effectively increased the concentration of activatable Qo sites when the Complex is partly reduced.

These simulations show that distances between redox centers in Complex III have been selected to be short enough to permit rapid enough inherent tunneling rates to allow millisecond catalysis at the Qo site, despite endergonic reactions associated with Qo catalysis, and to guide electrons in opposite directions from the Qo catalytic site to implement energy conversion. At the same time, distances have been selected to be long enough to minimize the problem of short-circuit energy wasting reactions. This is most clearly seen in the near perfect alignment of the three redox centers that make up the Qo catalytic site, FeS, Qo and heme b_L. The distances between Qo and its two redox partners at about 7 and 12 Å are relatively short, so catalysis is fast enough; however, the direct distance between heme b_L and FeS at 23 Å is nearly as long as possible given the first two distance constraints. Thus, direct short-circuit reactions that do not involve semiquinone and would be a danger even to a concerted Qo catalysis mechanism are minimized as much as possible. The distance between the two b_L hemes in a dimer also

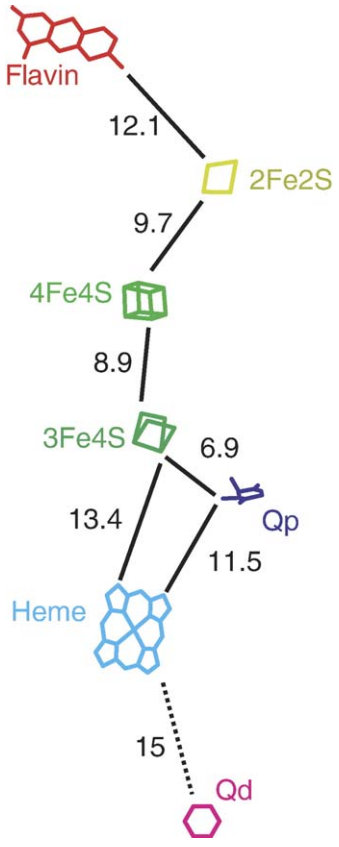

Fig. 6. Edge-to-edge distances between pairs of redox co-factors in Complex II taken from PDB structure file 1ZOY of pig heart succinate dehydrogenase at 2.4 Å resolution [37]. The distal quinone (Qd) is missing from the structure but the site is well enough defined to obtain a tunneling distance from the heme.

appears to be selected to be short enough to allow physiologically meaningful communication with redox species present in the other half of the dimer, which under certain redox conditions will stimulate catalytic turnover without the extra cost of synthesizing more complexes.

2.4. Complex II: succinate ubiquinone oxidoreductase

Complex II shuttles two electrons from its water-soluble substrate succinate to a membrane-soluble reduced ubiquinone product at 111 s^{-1} in the *B. taurus* mitochondrial protein [36]. Complex II apparently plays a unique regulatory role in setting the rate of respiration because it couples the state of reduction of quinone in the respiratory chain with the operation of the Krebs cycle where succinate and NADH are produced [37]. Unlike Complexes I, III, and IV, Complex II has no proton-pumping requirements tied to this transfer of electrons (Fig. 1); this absence of energy coupling demands, along with the generally linear configuration of its redox couples, make short-circuits a non-issue. The chain starts with covalently bound FAD acting as the initial two-electron acceptor; electrons are passed through three iron–sulfur clusters before entering the membranous domain, which contains a *b* heme and at least one ubiquinone binding site. The recent availability of high-resolution mitochondrial Complex II structures [37] have made it possible to accurately measure the inter-cofactor distances (Fig. 6). This information, coupled with experimentally determined redox midpoints (Tables 1 and 2), makes it possible to calculate the rates of electron tunneling and quinone reduction.

Fig. 7A shows a simulation of tunneling limited electron transfer reactions from reduced flavin to quinone in an otherwise oxidized complex. If flavin oxidation were limited by electron tunneling, the adjacent [2Fe2S] center should be reduced on a microsecond timescale. Further electron transfer is rate limited by the uphill electron transfer between [2Fe2S] and [4Fe4S]. [2Fe2S] should succeed in reducing the [4Fe4S] with subsequent rapid downhill electron tunneling to 3Fe4S and the adjacent quinone on a 300 -μs timescale. Thus, the network of electron tunneling reactions in Complex II is more than an order of magnitude faster than the 10 ms catalytic turnover [36], which is likely to be limited by bond-making and -breaking reactions at the succinate and quinone catalytic sites. The log K_{stab} for the quinone could be lowered from the observed mildly unstable −1.3 to a significantly more unstable −7 while still keeping the tunneling rate to the quinone faster than the catalytic turnover rate. The sub-millisecond tunneling rates between redox centers in the tunneling simulation are comparable to sub-millisecond intraprotein electron transfer rates in Complex II observed by pulse radiolysis [38]. The b heme, which has a significantly lower redox potential in mitochondria compared to many bacteria, is essentially uninvolved in these millisecond timescale electron transfer simulations of the oxidized enzyme.

However, Fig. 7A also shows that on a seconds timescale there is the beginning of electron equilibration between the quinone resolved in the mitochondrial structure (Qp) and another site about 15Å away from the b heme towards the opposite side of the membrane [37]. Although there is no quinone resolved in this mitochondrial site, it is in a location analogous to the second clearly resolved quinone in bacterial structures [39]. According to early redox titrations of semiquinone in Complex II [40], there are two semiquinones with similar redox properties. These may not correspond to Qp and Qd, as the EPR distance between the two semiquinones was estimated at ~8 Å compared to the ~32 Å between the two sites indicated by the structure. However, in the absence of other quinone redox midpoint measurements in Complex II, we set the redox properties of the Qp and Qd to be identical in the simulations. At sufficiently long times, these simulations show electron tunneling redox equilibration between the two quinones.

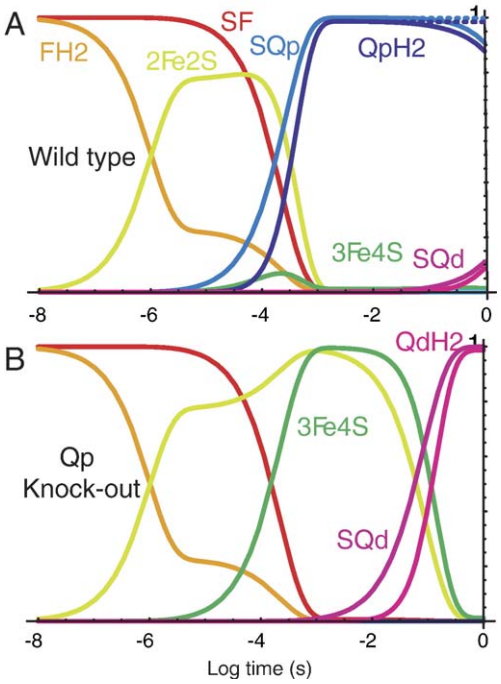

Fig. 7. Mitochondrial succinate dehydrogenase electron tunneling simulations. (A) Idealized tunneling limited electron transfer from reduced flavin through an oxidized enzyme to the nearest quinone. Knocking-out the heme has little effect except at long timescales (dashed lines). (B) Analogous electron tunneling when reduction to the nearest quinone has been blocked (e.g., with an inhibitor) revealing the ability to reduce the distance quinone, via transient reduction of the heme, on a 100-ms timescale.

The heme, which is relatively uninvolved in the reduction of the first quinone, is clearly important in equilibration between the two quinones, which should take place on the seconds timescale. Fig. 7B shows the effect of removing the near quinone Qp, to reveal the inherent tunneling rates through the heme to the distal quinone Qd, on a ~100 ms timescale, slightly slower than the observed turnover rate of the enzyme [36]. Knocking-out the heme slows this equilibration by orders of magnitude (dashed lines of Fig. 7A). Although heme knock-outs have been created in Complex III, the analogous knock-outs in Complex II so far appear to interfere with assembly of the enzyme [41,42] so that a functional knock-out might best be achieved by an incapacitating dramatic change of lowering the heme redox potential, rather that removing heme ligation, as has been done with heme c_1 in Complex III [43].

Although these tunneling simulations show that heme mediated distal quinone reduction is possible, it is difficult to see how this quinone reduction could be an advantage to the organism. Both the transmembrane electron transfer and the absorption of protons from the cytoplasmic aqueous phase during distal quinone reduction would compromise the transmembrane potential and proton gradient produced by normal respiration of the other complexes (Fig. 1). On the other hand, the reverse reaction, distal quinone oxidation and succinate reduction to fumarate, would add to the transmembrane potentials if Qp were effectively inoperative. Conceivably the distal quinone and reverse reaction could be part of Complex II's regulatory role in coupling the mitochondrial bioenergetic state with the Krebs cycle. Then again, the quinone may be merely a vestige of ancient operation of the precursors of the modern mitochondrial enzyme. There are bacterial analogues of this enzyme with higher heme potentials that can operate in this "reverse" direction.

Because the heme cannot be reduced by succinate, but can be oxidized by fumarate [44], there has been some speculation that the heme participates only in physiological reverse reactions. Rather than evidence for mechanistic complexity or irreversibility, these observations are a simple consequence of the equilibrium redox potentials of the heme (−0.185 V) and the succinate fumarate couple (+0.025 V [45]) which favors heme to fumarate electron transfer rather than the reverse.

Although the Qo site of Complex III and the Qp site of Complex II are in different complexes and on different sides of the membrane, they share some remarkable similarities. They have not only the same classes of redox partners, FeS and heme, but virtually the same tunneling distances to these centers. However, Complex II, with no danger of short-circuit, tolerates a direct heme to FeS distance much smaller than the comparable distance in Complex III (13.4 vs. 23.9 Å). This shorter distance is what makes direct electron transfer practical and indicates that the reverse transmembrane electron transfer from Qd to [3Fe4S] is a real possibility.

2.5. Complex I: NADH ubiquinone oxidoreductase

Although the molecular mechanism is largely unknown, Complex I turns the 0.82 V of standard free energy for 2 electrons moving from NADH to ubiquinone into a transmembrane translocation of 4 protons and 4 charges [46], compared to 2 protons with 4 charges translocated by the 1.1 V of standard free energy provided by two electrons in Complex IV [47]. Certain membranous subunits of Complex I are related to bacterial transmembrane cation/proton antiport proteins, supporting the general consensus is that, like Complex IV, there is some sort of proton pumping mechanism supporting the proton to electron stoichiometery [48–50]. However, the lack of a high-resolution structure for the membrane domain of mitochondrial Complex I makes these issues difficult to resolve.

There is a crystal structure of the water soluble domain of Complex I in *Thermus thermophilus* which has sufficient resolution to locate the FeS clusters [51,52]. All the FeS centers and the flavin are in the non-membranous domain, which makes it unlikely that they are directly involved in proton pumping. The structure also includes an additional FeS cluster (N7) not found in the mitochondrial complex (Fig. 8). Quinone is not resolved in this structure, but distance estimates are available from EPR spin interactions [49,53]. With these distances, we can use a tunneling analysis to look at the action of a chain more than 80Å long that, like Complex II, connects two 2-electron centers by a chain of 1-electron centers (Fig. 9).

Without a structural resolution of where NADH is located, the electron transfer simulation begins with reduced flavin. Flavin has a marginally unstable semiquinone state [54], but the fully reduced flavin to semiquinone couple has more than enough reducing power to reduce nearby N3, with electron tunneling expected on a nanosecond timescale, assuming that there are no proton transfer limiting steps in flavin oxidation that would slow down the electron transfer reactions (Fig. 9A). By half a microsecond N3 releases an electron to N1b and picks up the second electron from the flavin. By 5 ms, the two electrons are expected to be evenly distributed among the isopotential centers N3, N1b, N4 and N5 and some equilibration with the remote N1a center near the flavin. There is a relatively long 14 Å gap between N5 and the next N6 (a or b) in the chain, so there is a tens of microseconds delay expected before the other iron sulfur centers receive electrons. However, if the quinone redox couple is sufficiently oxidizing, then after electrons cross this gap to N6, the subsequent electron transfer through the unusually oxidizing center N2 onto the quinone would follow in rapid succession, so that N6 centers and N2 are reduced only transiently. Center N7, which is a long 21Å away, is not involved on this timescale.

The redox couples of quinone in Complex I are unknown. Although the semiquinone can be observed by EPR spectroscopy, which allows the distance from N2 to be estimated, so far it can only be observed under applied membrane potential and not in an equilibrium redox titration. Thus, even the average Q/QH_2 redox couple of this quinone is unknown. Because a Qnf semiquinone

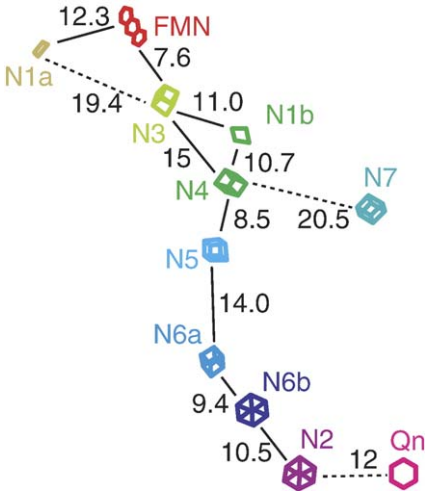

Fig. 8. Complex I edge-to-edge distances as reported for a crystal structure from *T. thermophilus* [51,52]. Quinone [49,62] distance not resolved in this crystal structure are estimated from EPR spin distances. Mitochondrial Complex I does not include center N7. Centers N4 and N5 are located based on the ligand arrangements in the solved structure [52]. The ordering of N6a and N6b are arbitrary.

signal can appear in up to half the Complex I, it appears that the semiquinone may be moderately stable under energized conditions. Under non-energized conditions the semiquinone is unobservable, suggesting that K_{stab} is much less than one. If we use the hypothetical Qnf redox couples for the stable semiquinone recently suggested by Ohnishi and Salerno [49] (Fig. 9A, solid lines), tunneling limited rates indicate that semiquinone would be formed 50 μs after flavin oxidation. After the quinone is mostly reduced to the semiquinone, then N2 can start to accumulate electrons and share them with the nearly equipotential SQ/QH_2 redox couple on the 100 μs timescale. Using the hypothetical more oxidizing and unstable semiquinone redox couples suggested by Ohnishi and Salerno for the non-membrane-energized condition (Fig. 9A dashed) delays semiquinone formation, but fully reduced QH_2 would form on the same timescale, with nearly complete electron transfer and very little reduced N2 appearing even transiently.

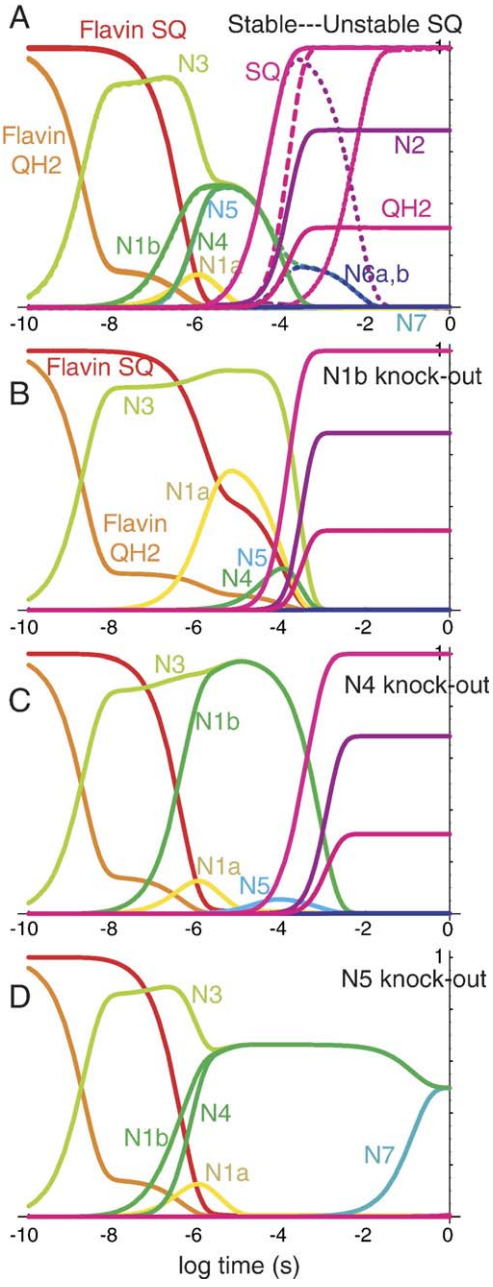

Fig. 9. Electron tunneling network simulations of Complex I, beginning with reduced flavin and all other centers oxidized. (A) Electron tunneling reactions are fast enough to support the catalytic turnover rate of the enzyme when redox couples for quinone favor semiquinone (solid lines), mildly disfavor (dashed), or even when semiquinone is highly disfavored with a log K_{stab} of −14 (dotted). (B–D) A simulation of single knock-outs of FeS centers, N1b, N4 and N5, respectively. While the first two knock-outs can support catalytic turnover rates, the N5 knock-out reduces quinone only on an hour timescale.

Each of these quinone reduction rates is much faster than the catalytic turnover of the enzyme; thus semiquinone Qnf could be considerably more unstable and more like the Qo of Complex III, still allowing rapid enough reduction by tunneling from N2 to support the observed catalytic turnover of 100–150 s^{-1} [55]. For example, if the log K_{stab} were −14 (dotted lines of Fig. 9A), then the simulations indicate that electrons would accumulate on N2 until it was nearly fully reduced, N6a and b would also appear partly reduced, and Qn would become doubly reduced on the 5 ms catalytic turnover timescale.

There are some important mechanistic consequences to the possibility that at least one quinone in Complex I may have a very low stability constants. For example, with a log K_{stab} of −14, as in Fig. 9A, the two quinone redox couples will be separated by a large 0.84V. This means that if the quinone were to have the average redox properties of pool quinone, the Q/SQ couple would be around −0.33V — low, but reducible by flavin. The other SQ/QH_2 couple would be around +0.51V, providing an astonishing 0.83 eV of driving force for electron transfer. This should be more than enough to drive the proton pumping mechanism of Complex I. Furthermore, in quinone redox chemistry, the reduction of the second couple is often associated with the uptake of two protons: $SQ + e^- + 2H^+ \rightarrow QH_2$. We have described [48] a pump mechanism for Complex I that exploits this second, high driving force redox couple as a non-exchangeable quinone that engages in proton uptake, conformational changes and proton pumping to achieve the 4 proton, 4 transmembrane charge translocation per 2 electron stoichiometry of Complex I. Under equilibrium redox titrations, the semiquinone of this species would not appear, because the K_{stab} is so low. However, under energized turnover conditions, after the quinone is primed with an electron to form the semiquinone state, it may become visible by EPR, thereafter actively moving between the SQ and QH_2 state. A similar mechanism has recently appeared that does not make explicit mention of the role of other quinones in Complex I [49]. It is of course also possible that proton pumping by Complex I exploits the large driving force of this second reduction of quinone, without relying directly on quinone to manage the pumped protons.

Complex I has a cluster of FeS centers in the middle of the chain that would in principle tolerate cofactor dysfunction or knock-out and still have tunneling rates fast enough to support rapid catalytic turnover. If cofactor N1b were knocked out, Fig. 9B shows that flavin would reduce N3 as usual and significantly reduce N1a, but that the electron would not progress down the chain until about 100 μs, transiently appearing on N4 and N5 before going on to form semiquinone. The second electron would then pause at N3 before passing quickly through the N5, N4 relay to partly reduce centers N2 and QH_2 on a 200-μs timescale. This is

only about 10 times slower than the wild-type with N1b active. By knocking-out of the N4 cofactor instead, electron transfer would slow a bit more (Fig. 9C). Now that two FeS centers N3 and N1b are available, flavin would double oxidize as usual, but electron transfer through N5 to form semiquinone would be delayed until 200 μs and accumulation of electrons on N2 and QH_2 would be on the millisecond timescale. The knock-out of cofactor N5 (Fig. 9D) leaves a big gap in the chain and is clearly lethal, with electrons accumulating on the isopotential FeS centers N3, N1b and N4 and remaining there for 100 ms until the distant isopotential [56,57] N7 FeS center in bacterial Complex I begins to share the electron. Center N7 effectively acts as a high impedance, long time-constant monitor of the state of reduction of the reducing end of the Complex I electron transport chain. Reduction of the quinone in this N5 knock-out simulation takes almost an hour.

Distances between cofactors in Complex I are selected to be short enough to easily allow electron transfer down this unusually long chain in a time securely faster than that required to support catalytic turnover of the enzyme. While the more than 80 Å distance seems absurdly long for the simple act of connecting two catalytic centers, this design may reflect the modular origin of modern respiratory Complex I from hydrogenase-like and other enzymatic ancestors [58]. If this was the case, the distances between redox centers which worked for the earlier enzymatic functions were, not surprisingly, also entirely adequate when subunits were concatenated to make a longer chain in Complex I. The major concern on connecting modules would be keeping the cofactor distances at the interface at 14Å or less, which seems to have been satisfied. The relatively long distances between chain elements and the catalytic sites of flavin and quinone reduction, compared to the catalytic cluster of Complex IV, suggest that the barriers for oxidation or reduction of these two electron centers may be relatively small; closely paired electron transfer reactions to accommodate a large uphill electron transfer step do not appear to be necessary in Complex I. The long distance between N2 and Qnf could be a problem for mechanisms that require the quinone to be intimately involved in a high barrier, short-circuit vulnerable energy coupling and proton pumping, which would have the effect of slowing the electron transfer rate. However, the Complex I structure is not completely resolved and other redox centers (such as Qns) need to be placed before we can consider the energy coupling mechanism further.

3. Conclusion

Each of the respiratory Complexes includes one or more chains of redox centers connected to one or more multi-electron catalytic sites. Depending upon the magnitude of the chemical barriers at the catalytic site, and the possibility of proton or electron short-circuiting, the distances between redox centers near the catalytic sites are either short, to cluster redox centers and provide rapid enough electron tunneling to scale barriers, or long, to weaken energy wasting short-circuit reactions. Table 3 summarizes the different constraints faced by each Complex, and the adjustment of tunneling distances in each case. The natural selection of distances in the appropriate range for these functions gives the Complexes a robustness in electron transfer rates that tolerates mutational changes in the protein and may have been essential for successful cycles of variation and selection that led to these modern forms of the respiratory Complexes.

Table 3
Distance related engineering issues that distinguish the complexes

Complex	Chain ($R<\sim14$Å)	Cluster barrier scaling ($R<<14$Å)	Short-circuit prevention ($R>14$Å)	Unstable substrate intermediate
IV	yes	yes, 4 e-	yes, H+ short	yes, O_2 couples
III	yes	yes, 2e-	yes, e- short	yes, Qo
II	yes	no	no	no
I	yes	probably not	yes, H+ short	no

Beyond the principle concern of setting electron tunneling distances, the heights of barriers at the catalytic sites is next in importance in the engineering of electron transfer proteins. An important contribution to the barrier at the various quinone catalytic sites is the potentially uphill electron transfer to and from the oxidizing and reducing redox couples of the quinone, as quantified by the K_{stab}. Most quinone sites are designed with redox partners at sufficiently short distances and appropriate redox potentials so that protein surrounding the quinone has the freedom to provide a wide range of stability constants and still allow electron tunneling not to be rate limiting for catalytic turnover. The Qo site in Complex III is the only Q site that actually requires a small K_{stab} and moderately large energetic barrier for electron tunneling because of its singular vulnerability to semiquinone mediated short-circuits, and is the only quinone site that clearly needs to be in a cluster. All other quinone sites have less unstable semiquinones and can tolerate long tunneling distances and do not require more than one close redox partner. It appears that in the design of quinone binding sites, it is sufficient for the protein to provide hydrogen bonding geometries or protonation partners that mildly stabilize the semiquinone and moderately raise the K_{stab} from the $\sim10^{-10}$ range of unbound quinone in the pool [27], to $\sim10^{-7}$ in the quinone binding sites.

Acknowledgements

Supported by U.S. Public Health Service Grant GM27309. We are grateful to Tomoko Ohnishi, University of Pennsylvania, for insightful discussions and clarification of Complex I and II quinone and FeS cluster properties and to Leonid Sazanov, University of Cambridge, for thoughtful discussion and early release of results.

References

[1] C.C. Page, C.C. Moser, X. Chen, P.L. Dutton, Natural engineering principles of electron tunneling in biological oxidation–reduction, Nature (London) 402 (1999) 47–52.
[2] R.A. Marcus, N. Sutin, Electron transfers in chemistry and biology, Biochim. Biophys. Acta 811 (1985) 265–322.
[3] M.R. Gunner, P.L. Dutton, Temperature and -delta-G-degrees dependence of the electron- transfer from Bph.- to Qa in reaction center protein from *Rhodobacter sphaeroides* with different quinones as Qa, J. Am. Chem. Soc. 111 (1989) 3400–3412.
[4] C.C. Moser, J.M. Keske, K. Warncke, R.S. Farid, P.L. Dutton, Nature of biological electron transfer, Nature (London) 355 (1992) 796–802.

[5] J.J. Hopfield, Electron transfer between biological molecules by thermally activated tunneling, Proc. Natl. Acad. Sci. U. S. A. 71 (1974) 3640–3644.
[6] M. Karpefors, P. Adelroth, A. Namslauer, Y.J. Zhen, P. Brzezinski, Formation of the "peroxy" intermediate in cytochrome *c* oxidase is associated with internal proton/hydrogen transfer, Biochemistry 39 (2000) 14664–14669.
[7] P. Adelroth, P. Brzezinski, B.G. Malmstrom, Internal electron transfer in cytochrome *c* oxidase from *Rhodobacter sphaeroides*, Biochemistry 34 (1995) 2844–2849.
[8] G.T. Babcock, M. Wikstrom, Oxygen activation and the conservation of energy in cell respiration, Nature 356 (1992) 301–309.
[9] M. Wikstrom, M.I. Verkhovsky, G. Hummer, Water-gated mechanism of proton translocation by cytochrome *c* oxidase, Biochim. Biophys. Acta, Bioenerg. 1604 (2003) 61–65.
[10] A. Osyczka, C.C. Moser, F. Daldal, P.L. Dutton, Reversible redox energy coupling in electron transfer chains, Nature 427 (2004) 607–612.
[11] M. Oliveberg, B.G. Malmstrom, Internal electron transfer in cytochrome *c* oxidase: evidence for a rapid equilibrium between cytochrome a and the bimetallic site, Biochemistry 39 (1991) 7053–7057.
[12] M.I. Verkhovsky, J.E. Morgan, M. Wikstrom, Intramolecular electron transfer in cytochrome *c* oxidase: a cascade of equilibria, Biochemistry 31 (1992) 11860–11863.
[13] J.J. Regan, B.E. Ramirez, J.R. Winkler, H.B. Gray, B.G. Malmstrom, Pathways for electron tunneling in cytochrome *c* oxidase, J. Bioenerg. Biomembr. 30 (1998) 35–39.
[14] E. Pilet, A. Jasaitis, U. Liebl, M.H. Vos, Electron transfer between hemes in mammalian cytochrome *c* oxidase, Proc. Natl. Acad. Sci. U. S. A. 101 (2004) 16198–16203.
[15] M.I. Verkhovsky, A. Jasaitis, M. Wikstrom, Ultrafast haem–haem electron transfer in cytochrome *c* oxidase, Biochim. Biophys. Acta 1506 (2001) 143–146.
[16] P. Nicholls, J.M. Wrigglesworth, Routes of cytochrome a3 reduction — the neoclassical model revisited, Ann. N. Y. Acad. Sci. 550 (1988) 59–67.
[17] P. Mitchell, Protonmotive redox mechanism of the cytochrome b-c1 complex in the respiratory chain: protonmotive ubiquinone cycle, FEBS Lett. 56 (1975) 1–6.
[18] A.R. Crofts, S.W. Meinhardt, K.R. Jones, M. Snozzi, The role of the quinone pool in the cyclic electron-transfer chain of *Rhodopseudomonas sphaeroides*: a modified q-cycle mechanism, Biochim. Biophys. Acta 723 (1983) 202–218.
[19] B. Chance, A.R. Crofts, M. Nishimura, B. Price, Fast membrane H+ binding in the light-activated state of chromatium chromatophores, Eur. J. Biochem. 13 (1970) 364–374.
[20] D.E. Robertson, R.C. Prince, J.R. Bowyer, K. Matsuura, P.L. Dutton, T. Ohnishi, Thermodynamic properties of the semiquinone and its binding site in the Ubiquinol-Cytochrome c (c2) oxidoreductase of respiratory and photosynthetic systems, J. Biol. Chem. 259 (1984) 1758–1763.
[21] T. Ohnishi, B.L. Trumpower, Differential effects of antimycin on ubisemiquinone bound in different environments in isolated succinate-cytochrome *c* reductase complex, J. Biol. Chem. 255 (1980) 3278–3284.
[22] S. Junemann, P. Heathcote, P.R. Rich, On the mechanism of quinol oxidation in the bc1 complex, J. Biol. Chem. 273 (1998) 21603–21607.
[23] P.R. Rich, Electron and proton transfers through quinones and cytochrome-bc complexes, Biochim. Biophys. Acta 768 (1984) 53–79.
[24] H. Ding, C.C. Moser, D.E. Robertson, M.K. Tokito, F. Daldal, P.L. Dutton, Ubiquinone pair in the Qo site central to the primary energy conversion reactions of cytochrome bc1 complex, Biochemistry 34 (1995) 15979–15996.
[25] K. Takamiya, P.L. Dutton, Ubiquinone in *Rhodopseudomonas sphaeroides*. Some thermodynamic properties, Biochim. Biopphys. Acta 546 (1979) 1–16.
[26] K.-I. Takamiya, P.L. Dutton, Ubiquinone in *Rhodopseudomonas sphaeroides* some thermodynamic properties, Biochim. Biophys. Acta 546 (1979) 1–16.
[27] P. Mitchell, Possible molecular mechanisms of the protonmotive function of cytochrome systems, J. Theor. Biol. 62 (1976) 327–367.
[28] S. Iwata, J.W. Lee, K. Okada, J.K. Lee, M. Iwata, B. Rasmussen, T.A. Link, S. Ramaswamy, B.K. Jap, Complete structure of the 11-subunit bovine mitochondrial cytochrome bc1 complex, Science 281 (1998) 64–71.
[29] H. Kim, D. Xia, C.A. Yu, J.Z. Xia, A.M. Kachurin, L. Zhang, L. Yu, J. Deisenhofer, Inhibitor binding changes domain mobility in the iron–sulfur protein of the mitochondrial bc1 complex from bovine heart, Proc. Natl. Acad. Sci. U. S. A. 95 (1998) 8026–8033.
[30] Z. Zhang, L. Huang, V.M. Shulmeister, Y.-I. Chi, K.K. Kim, L.-W. Hung, A.R. Crofts, E.A. Berry, S.H. Kim, Electron transfer by domain movement in cytochrome bc1, Nature 392 (1998) 677–684.
[31] R.C. Sadoski, G. Engstrom, H. Tian, L. Zhang, C.A. Yu, L. Yu, B. Durham, F. Millett, Use of a photoactivated ruthenium dimer complex to measure electron transfer between the Rieske iron–sulfur protein and cytochrome *c*(1) in the cytochrome bc(1) complex, Biochemistry 39 (2000) 4231–4236.
[32] P.R. Rich, A.E. Jeal, S.A. Madgwick, A.J. Moody, Inhibitor effects on Redox-linked protonations of the B-hemes of the mitochondrial-Bc1 complex, Biochim. Biophys. Acta 1018 (1990) 29–40.
[33] J.N. Siedow, S. Power, F.F. de la Rosa, G. Palmer, The preparation and characterization of highly purified, enzymically active complex III from Baker's Yeast, J. Biol. Chem. 253 (1978) 2392–2399.
[34] F.F. de la Rosa, G. Palmer, Reductive titration of CoQ-depleted complex III from Baker's Yeast: evidence for an exchange-coupled complex between QH. and Low-spin Ferricytochrome b, FEBS Lett. 163 (1983) 140–143.
[35] A. Osyczka, C.C. Moser, P.L. Dutton, Fixing the Q Cycle, Trends Biochem. Sci. 30 (2005) 176–182.
[36] G. Cecchini, I. Schroder, R.P. Gunsalus, E. Maklashina, Succinate dehydrogenase and fumarate reductase from *Escherichia coli*, Biochim. Biophys. Acta, Bioenerg. 1553 (2002) 140–157.
[37] F. Sun, X. Huo, Y.J. Zhai, A.J. Wang, J.X. Xu, D. Su, M. Bartlam, Z.H. Rao, Crystal structure of mitochondrial respiratory membrane protein complex II, Cell 121 (2005) 1043–1057.
[38] R.F. Anderson, R. Hille, S.S. Shinde, G. Cecchini, Electron transfer within complex II - succinate: ubiquinone oxidoreductase of *Escherichia coli*, J. Biol. Chem. 280 (2005) 33331–33337.
[39] T.M. Iverson, C. Luna-Chavez, G. Cecchini, D.C. Rees, Structure of the *Escherichia coli* fumarate reductase respiratory complex, Science 284 (1999) 1961–1966.
[40] W.J. Ingledew, J.C. Salerno, T. Ohnishi, Studies on electron-paramagnetic resonance-spectra manifested by a respiratory-chain hydrogen carrier, Arch. Biochem. Biophys. 177 (1976) 176–184.
[41] L. Hederstedt, L. Rutberg, Biosynthesis and membrane-binding of succinate-dehydrogenase in *Bacillus subtilis*, J. Bacteriol. 144 (1980) 941–951.
[42] L. Hederstedt, Succinate: quinone oxidoreductase in the bacteria *Paracoccus denitrificans* and *Bacillus subtilis*, Biochim. Biophys. Acta, Bioenerg. 1553 (2002) 74–83.
[43] A. Osyczka, C.C. Moser, P.L. Dutton, Novel cyanide inhibition at cytochrome *c*1 of *Rhodobacter capsulatus* cytochrome bc1, Biochim. Biophys. Acta 1655 (2004) 71–76.
[44] J. Peterson, C. Vibat, R.B. Gennis, Identification of the axial heme ligands of cytochrome B(556) in succinate-ubiquinone oxidoreductase from *Escherichia coli*, FEBS Lett. 355 (1994) 155–156.
[45] H. Borsook, H. Schott, The role of the enzyme in the enzyme-fumarate equilibrium, J. Biol. Chem. 92 (1931) 535–557.
[46] M. Wikstrom, 2 Protons are pumped from the mitochondrial matrix per electron transferred between NADH and ubiquinone, FEBS Lett. 169 (1984) 300–304.
[47] P.L. Dutton, T. Ohnishi, E. Darrouzet, M.D. Leonard, R.E. Sharp, B.R. Gibney, F. Daldal, in: P. Quinn, V. Kagan (Eds.), Coenzyme Q: From Molecular Mechanisms to Nutrition and Health, CRC Press Publishers, Florida, 2000, pp. 65–82.
[48] P.L. Dutton, C.C. Moser, V.D. Sled, F. Daldal, T. Ohnishi, A reductant-induced oxidation mechanism for Complex I, Biochim. Biophys. Acta 1364 (1998) 245–257.
[49] T. Ohnishi, J.C. Salerno, Conformation-driven and semiquinone-gated proton-pump mechanism in the NADH-ubiquinone oxidoreductase (complex I), FEBS Lett. 579 (2005) 4555–4561.
[50] T. Ohnishi, J.C Salerno, in: T.G. Spiro (Ed.), Iron–Sulfur Proteins, Wiley, New York, 1982, pp. 285–327.
[51] P. Hinchliffe, L.A. Sazanov, Organization of iron–sulfur clusters in respiratory complex I, Science 309 (2005) 771–774.
[52] L.A. Sazanov, P. Hinchliffe, Structure of the hydrophilic domain of respiratory complex I from *Thermus thermophilus*, Science 311 (2006) 1430–1436.

[53] T. Ohnishi, in: R.A. Capaldi (Ed.), Membrane Proteins in Energy Transduction, Marcel Dekker Inc., New York, 1979, pp. 1–87.
[54] R. Horsefield, S. Iwata, B. Byrne, Complex II from a structural perspective, Curr. Prot. Peptide Sci. 5 (2004) 107–118.
[55] C.I. Ragan, E. Racker, Resolution and reconstitution of mitochondrial electron-transport system.4. reconstitution of rotenone-sensitive reduced nicotinamide adenine dinucleotide-ubiquinone reductase from reduced nicotinamide adenine-dinucleotide dehydrogenase and phospholipids, J. Biol. Chem. 248 (1973) 6876–6884.
[56] M. Uhlmann, T. Friedrich, EPR signals assigned to Fe/S cluster N1c of the *Escherichia coli* NADH: ubiquinone oxidoreductase (Complex I) derive from cluster N1a, Biochemistry 44 (2005) 1653–1658.
[57] E. Nakamaru-Ogiso, T. Yano, T. Yagi, T. Ohnishi, Characterization of the iron–sulfur cluster N7 (N1c) in the subunit NuoG of the proton-translocating NADH-quinone oxidoreductase from *Escherichia coli*, J. Biol. Chem. 280 (2005) 301–307.
[58] T. Friedrich, H. Weiss, Modular evolution of the respiratory NADH: ubiquinone oxidoreductase and the origin of its modules, J. Theor. Biol. 187 (1997) 529–540.
[59] L. Banci, I. Bertnini, J.G. Huber, G.A. Spyroulias, P. Turano, Solution structure of reduced horse heart cytochrome *c*, J. Biol. Inorg. Chem. 4 (1999) 21–31.
[60] T. Tsukihara, H. Aoyama, E. Yamashita, T. Tomizaki, H. Yamaguchi, K. ShinzawaItoh, R. Nakashima, R. Yaono, S. Yoshikawa, The whole structure of the 13-subunit oxidized cytochrome *c* oxidase at 2.8 angstrom, Science 272 (1996) 1136–1144.
[61] S. Yoshikawa, K. Shinzawa-Itoh, R. Nakashima, R. Yaono, E. Yamashita, N. Inoue, M. Yao, M.J. Fei, C.P. Libeu, T. Mizushima, H. Yamaguchi, T. Tomizaki, T. Tsukihara, Redox-coupled crystal structural changes in bovine heart cytochrome *c* oxidase, Science 280 (1998) 1723–1729.
[62] T. Yano, W.R. Dunham, T. Ohnishi, Characterization of the Delta mu(H)+-sensitive ubisemiquinone species (SQ(Nf)) and the interaction with cluster N2: new insight into the energy-coupled electron transfer in complex I, Biochemistry 44 (2005) 1744–1754.
[63] T. Ohnishi, Iron–sulfur clusters semiquinones in Complex I, Biochim. Biophys. Acta, Bioenerg. 1364 (1998) 186–206.
[64] B.L. Trumpower, Function of the iron–sulfur protein of the cytochrome-b–c1 segment in electron-transfer and energy-conserving reactions of the mitochondrial respiratory-chain, Biochim. Biophys. Acta 639 (1981) 129–155.
[65] A.J. Moody, P.R. Rich, The effect of pH on redox titrations of haem a in cyanide-liganded cytochrome *c* oxidase: experimental and modelling studies, Biochim. Biophys. Acta 1015 (1990) 205–215.
[66] T. Rasmussen, D. Scheide, B. Brors, L. Kintscher, H. Weiss, T. Friedrich, Identification of two tetranuclear FeS clusters on the ferredoxin-type subunit of NADH: ubiquinone oxidoreductase (complex I), Biochemistry 40 (2001) 6124–6131.
[67] C. Tommos, J.J. Skalicky, D.L. Pilloud, C.C. Moser, A.J. Wand, P.L. Dutton, De novo proteins designed to study properties of redox-active amino acids, J. Inorg. Biochem. 74 (1999) 316.
[68] T. Ohnishi, J.C. Salerno, D.B. Winter, J. Lim, C.A. Yu, L. Yu, T.E. King, Thermodynamic and Epr characteristics of 2 ferredoxin-type iron–sulfur centers in succinate ubiquinone reductase segment of respiratory-chain, J. Biol. Chem. 251 (1976) 2094–2104.
[69] T. Ohnishi, J. Lim, D.B. Winter, T.E. King, Thermodynamic and Epr characteristics of a hipip-type iron–sulfur center in succinate-dehydrogenase of respiratory-chain, J. Biol. Chem. 251 (1976) 2105–2109.
[70] L. Yu, J.X. Xu, P.E. Haley, C.A. Yu, Properties of bovine heart mitochondrial cytochrome-B560, J. Biol. Chem. 262 (1987) 1137–1143.
[71] V.D. Sled, N.I. Rudnitzky, Y. Hatefi, T. Ohnishi, Thermodynamic analysis of flavin in mitochondrial NADH-Ubiquinone Oxidoreductase (Complex-I), Biochemistry 33 (1994) 10069–10075.
[72] T. Ohnishi, T.E. King, J.C. Salerno, H. Blum, J.R. Bowyer, T. Maida, Thermodynamic and electron-paramagnetic resonance characterization of flavin in succinate-dehydrogenase, J. Biol. Chem. 256 (1981) 5577–5582.
[73] T.T. Ohnishi, B.L., Differential effects of antimycin on ubisemiquinone bound in different environments in isolated succinate-cytochrome *c* reductase complex, J. Biol. Chem. 255 (1985) 3278–3284.